Journal of The Electrochemical Society, **157** (9) F116-F123 (2010)
0013-4651/2010/157(9)/F116/8/$28.00 © The Electrochemical Society

Carbon Paste Gold Nanoparticles Sensor for the Selective Determination of Dopamine in Buffered Solutions

Nada F. Atta,[z] Ahmed Galal, Fekria M. Abu-Attia, and Shereen M. Azab

Department of Chemistry, Faculty of Science, University of Cairo, Giza 12613, Egypt

An effective electrochemical sensor for the selective determination of dopamine (DA) in the presence of ascorbic acid (AA) and uric acid (UA) in 0.04 mol L^{-1} universal buffer solution (pH 7.4) is introduced. The sensor is based on a carbon paste (CP) electrode modified with gold nanoparticles. In a mixture of DA, AA, and UA, the sensor shows high selective response toward DA and no response for AA or UA. The effect of various experimental parameters including time of deposition of gold nanoparticles on the CP electrode, pH, and scan rate on the voltammetric response of DA was investigated. At the optimum conditions, the concentration of DA was determined using differential pulse voltammetry in a linear range of 1.0×10^{-7} to 5.0×10^{-6} mol L^{-1} and 5.0×10^{-6} to 1.3×10^{-4} mol L^{-1} with correlation coefficients of 0.9995 and 0.9988 and a detection limit of 5.9×10^{-9} and 8.2×10^{-8} mol L^{-1}, respectively. The modified electrode can be used for the determination of DA spiked into human serum samples, and excellent recovery results were obtained over a wide concentration range of DA. Moreover, validation parameters, such as reproducibility, sensitivity, and recovery were evaluated successfully in the determination of DA in diluted human urine.
 [DOI: 10.1149/1.3456629]

Manuscript submitted February 12, 2010; revised manuscript received April 26, 2010. Published July 16, 2010.

Dopamine (DA) is one of the important neurotransmitters that are widely distributed in the mammalian central nervous system for message transfer. It plays a very important role in the functioning of central nervous, renal, hormonal, and cardiovascular systems.[1] Abnormal levels of DA lead to brain disorders such as Parkinson and schizophrenia diseases.[2-4] Uric acid (UA) is another important biomolecule present in urine and blood. It is a primary end product of purine metabolism. Its abnormal concentration levels lead to several diseases such as hyperuricaemia and gout.[5,6] Ascorbic acid (AA) is a vital component in human diet and is present in both animal and plant kingdoms.[7] Usually, AA, DA, and UA coexist in our body fluids and therefore selective determination of these molecules is very important from the clinical point of view. At bare electrodes, the selective determination of AA, DA, and UA is impossible because their oxidation potentials are very close. Besides, stability and reproducibility cannot be achieved at bare electrodes due to the surface fouling caused by the adsorption of oxidized products of AA on electrode surface.[8] Paracetamol or acetaminophen (ACOP) is a widely used over-the-counter analgesic (pain reliever) and antipyretic (fever reducer). It is commonly used for the relief of fever, headaches, and other minor aches and pains and is a major ingredient in numerous cold and flu remedies. Paracetamol is also used in the management of more severe pain (such as postoperative pain).[9] Carbon paste (CP) electrode, which is made up of carbon particles and organic liquid, has been widely applied in the electroanalytical community due to its low cost, ease of fabrication, high sensitivity for detection, and renewable surface.[10-14]

Electrodeposition of gold nanoparticles onto the surface of the CP electrode was another strategy to enhance the sensitivity of the immunosensor. Several research works had been conducted to construct a CP electrode modified with gold nanoparticles to be used as an immunosensor for the determination of α-fetoprotein,[15] carcinoma antigen,[16] or in streptavidin–biotine interaction,[17] or as enzyme biosensors,[18] also in the determination of hypoxanthine,[19] sulfur-containing compounds,[20] and homocysteiene.[21] The electrodeposition of gold nanoparticles onto other surfaces such as glassy carbon in sensing of allergen–antibody interaction[22] and acetylcholine esterase–choline oxidase[23] were examined. Monitoring of silver and gold electrodeposition on glassy carbon and silicon,[24] screen-printed,[25] and indium tin oxide surfaces[26-31] were also studied. Also, gold and gold–platinum alloy nanoparticles were electrodeposited on multiwalled carbon nanotubes for investigation of direct electron transfer of glucose oxidase[32] and for nitrite oxidation,[33] respectively. Simultaneous electrochemical determination of DA, AA, and UA was studied using different modified electrodes such as poly(acid chrome blue K) modified glassy carbon electrode,[34] CP electrode modified with tin hexacyanoferrate,[35] nano-Au self-assembled glassy carbon electrode,[36] and recently by modifying Pt or conducting polymer surfaces by Pd or Pt nanoparticles.[37-40]

In this study, an electrochemical sensor based on gold nanoparticles and graphite was constructed for the selective determination of DA. The gold nanoparticles on the surface of the electrode amplified the signal significantly. Moreover, the sensor showed sensitive and selective determination of DA in the presence of AA and UA.

Experimental

Materials and reagents.— DA, AA, UA and ACOP were purchased from Aldrich and were used as received. Britton–Robinson (B–R) (4.0×10^{-2} mol L^{-1}) buffer solution of pH 2–11 ($CH_3COOH + H_3BO_3 + H_3PO_4$) and phosphate buffer saline (PBS, pH 7.4, 137 mmol L^{-1} NaCl, 2.7 mmol L^{-1} KCl, 87 mmol L^{-1} Na_2HPO_4, and 14 mmol L^{-1} KH_2PO_4) were used as the supporting electrolytes. pH was adjusted using 0.2 mol L^{-1} NaOH. All solutions were prepared from analytical grade chemicals and sterilized Milli-Q deionized water.

Construction of gold nanoparticles modified CP electrode.— A CP electrode with a diameter of 3 mm was fabricated as described elsewhere[41] then was immersed into a 6 mmol L^{-1} hydrogen tetrachloroaurate ($HAuCl_4$) solution containing 0.1 mol L^{-1} KNO_3 (prepared in doubly distilled water and deaerated by bubbling with nitrogen). A constant potential of −0.4 V vs Ag/AgCl was applied for 400 s. The surface coverage of gold nanoparticles was 2.05×10^{-6} mol cm^{-2}. Then, the modified electrode (GNMCPE) was washed with doubly distilled water and dried carefully by a paper without touching the surface and then left to dry in air for 10 min before being used.

Instrumental and experimental setups.— Electrochemical measurements.— All voltammetric measurements were performed using a personal computer-controlled AEW2 electrochemistry work station and data were analyzed with an EC_{prog3} electrochemistry software, manufactured by Sycopel Scientific Limited (Tyne & Wear, U.K.). The one compartment cell with the three electrodes was connected to the electrochemical workstation through a C_3 stand from BAS. A platinum wire from BAS was employed as auxiliary electrode. All the cell potentials were measured with respect to Ag/AgCl (3 mol L^{-1} NaCl) reference electrode from BAS. One compartment glass cell (15 mL) fitted with a gas bubbler was used for electrochemical measurements. Solutions were degassed using pure nitrogen before and throughout the electrochemical measurements. A

[z] E-mail: Nada_fah1@yahoo.com

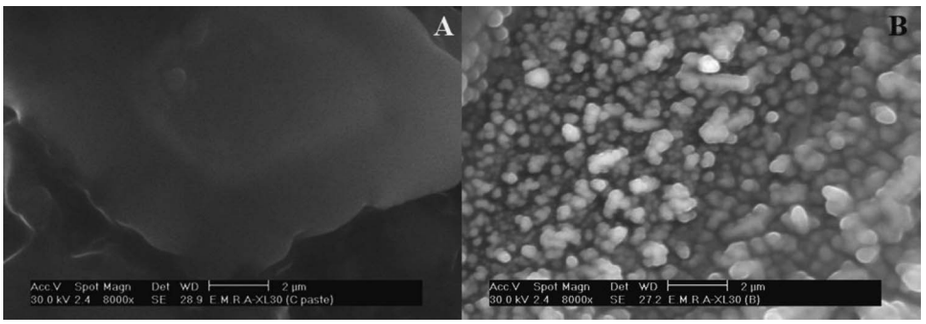

Figure 1. SEM of different electrodes: (A) CP electrode and (B) GNMCPE.

Jenway 3510 pH meter (England) with glass combination electrode was used for pH measurements. Scanning electron microscopy (SEM) measurements were carried out using a JSM-6700F scanning electron microscope (Japan Electro Co.). All the electrochemical experiments were performed at an ambient temperature of 25 ± 2°C.

Impedance spectroscopy measurements.— Electrochemical impedance spectroscopy (EIS) was performed using a Gamry-750 system and a lock-in amplifier that are connected to a personal computer. The data analysis software was provided with the instrument and applied a nonlinear least-squares fitting with the Levenberg–Marquardt algorithm. All impedance experiments were recorded between 0.1 Hz and 100 kHz with an excitation signal of 10 mV amplitude.

Analysis of serum.— Drug-free human blood, obtained from healthy volunteers, was centrifuged (5000 rpm) for 30 min at room temperature and the separated serum samples were stored frozen until the assay. An aliquot volume of the serum sample was fortified with DA dissolved in bidistilled water to achieve the final concentration of 1×10^{-3} mol L^{-1}. Acetonitrile removes serum proteins more effectively, as the addition of 1–1.5 vol is sufficient to remove the proteins. After vortexing for 30 s, the mixture was then centrifuged for 10 min at 5000 rpm to get rid of serum protein residues and supernatant liquid was taken carefully. Appropriate volumes of this supernatant liquid were transferred into the volumetric flask and diluted up to the marked volume with the B–R buffer of pH 7.4.

Analysis of urine.— Standard DA provided by the National Organization for Drug Control and Research of Egypt was dissolved in urine to make a stock solution with a 1.0×10^{-3} mol L^{-1} concentration. Standard additions of urine were carried out from a solution containing DA in 5 mL of B–R buffer pH 7.4.

Results and Discussion

Morphologies of the different electrodes.— The response of an electrochemical sensor was related to its physical morphology. The SEM of the CP electrode and GNMCPE are shown in Fig. 1. Significant differences in the surface structure of the CP electrode and GNMCPE were observed. The surface of the CP electrode was predominated by isolated and irregularly shaped graphite flakes and separated layers were noticed (Fig. 1A). The SEM image of the GNMCPE (Fig. 1B) shows that metallic nanoparticles are located at different elevations over the substrate. Moreover, a random distribution and interstices among the nanoparticles were observed in the SEM image of the GNMCPE exhibiting a large surface area.

Electrochemistry of DA at GNMCPE.— The voltammetric behavior of DA was examined using cyclic voltammetry (CV). Figure 2 compares typical cyclic voltammograms of 1.0×10^{-3} mol L^{-1} DA in B–R buffer pH 7.4 at a scan rate of 100 mV s^{-1} recorded at three different working electrodes (i.e., a bare CP, Au nanoparticles mixed with CP (AuNpCP), and GNMCPE electrodes). At the bare CP electrode and AuNpCP, the oxidation peak current was observed at 330 mV, whereas at the GNMCPE, the potential shifted negatively to 277 mV. Furthermore, for DA, an increase in peak current where GNMCPE was used was also observed due to the improvements in the reversibility of the electron transfer process and a larger real surface area of the modified electrode. The electrodeposition of Au particles on the CP electrode resulted in an observable increase in the peak current, which indicated an improvement in the electrode kinetics and a decrease in the potential of oxidation substantially (i.e., thermodynamically feasible reaction). The aforementioned results confirmed the key role played by Au nanoparticles on the catalytic oxidation of DA that acts as a promoter to enhance the electrochemical reaction.

Effect of operational parameters.— Effect of solution pH.— The effect of solution pH on the electrocatalytic oxidation of DA at the GNMCPE was studied by the cyclic voltammogram technique using B–R buffers within the pH range of 2–11 (Fig. 3). Both the anodic and the cathodic peak potentials shifted negatively with the increase in the solution pH, indicating that the electrocatalytic oxidation of DA at the GNMCPE is a pH-dependent reaction showing that protons have taken part in their electrode reaction processes. The relationship between the anodic peak potential and the solution pH value (over the pH range of 2–11) could be fit to the linear regression equation of $E_{pa}(V) = 0.675–0.0571$ pH, with a correlation coefficient of $r = 0.9927$. The slope was −57.1 mV/pH units over the pH range of 2–11, which is close to the theoretical value of −59 mV. This indicated that the number of protons and transferred electrons involved in the oxidation mechanism is equal.[42] As the DA oxidation is a two-electron process, the number of protons involved was also predicted to be two indicating a $2e^-/2H^+$ process. The peak current (Fig. 3, inset) decreased from pH 2 to pH 5 then increased at pH 6. At pH > 6, the peak current decreased again. Although the

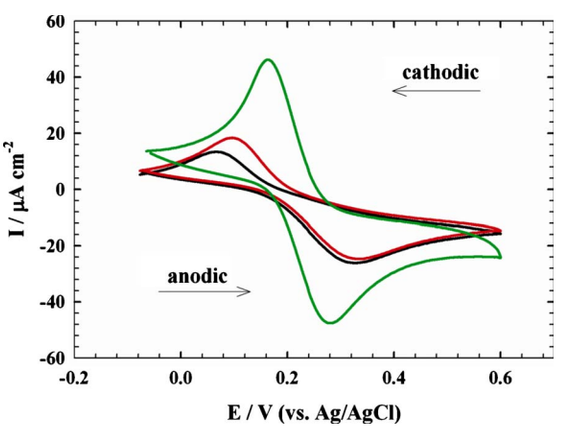

Figure 2. (Color online) Cyclic voltammograms of 1.0×10^{-3} mol L^{-1} DA in B–R buffer pH 7.4 at a scan rate of 100 mV s^{-1} recorded at three different working electrodes: [bare CP electrode (—), AuNpCP (red —), and GNMCPE (green —)].

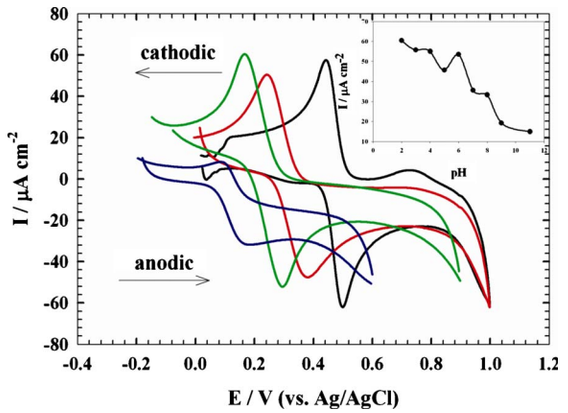

Figure 3. (Color online) Cyclic voltammetric response of 1.0 × 10^{-3} mol L^{-1} DA at the GNMCPE in 0.04 mol L^{-1} B–R buffers of different pH values [pH 2 (—), 5 (red —), 7 (green —), and 9 (blue —)]. The inset: Plot of the anodic peak current values vs pH values.

highest oxidation peak current was obtained at pH 2, other factors will be studied at pH 7.4 (i.e., pH medium of the human body).

Influence of the scan rate.— The effect of different scan rates on the current response was studied and a plot of i_{pa} vs $\nu^{1/2}$ (ν ranging from 10 to 250 mV s^{-1}) for DA (1.0 × 10^{-3} mol L^{-1}) on GNMCPE in the B–R buffer (pH 7.4) gave a straight line relationship. This revealed that the linearity of the relationship was realized up to a scan rate of 100 mV s^{-1} then followed by a deviation from linearity with the increasing scan rate. This indicated that the charge transfer was under diffusion control partially and that the adsorption of aggregates at the electrode surface was also possible. Typical CV curves of DA at different scan rates were shown in Fig. 4. It can be noticed that a pair of roughly symmetric anodic and cathodic peaks appeared with almost equal peak currents in the scan rate range from 10 to 100 mV s^{-1}. The peak-to-peak separation also increased with increasing the scan rate. A good linear relationship was found for the oxidation and the reduction peak currents, and different scan rates (Fig. 4 inset). The reduction and oxidation peak currents increased linearly with the linear regression equations as $i_{pc}(10^{-6}\ A) = 10.07\nu^{1/2}(V\ s^{-1})^{1/2} - 8.91(n = 5,\ \gamma = 0.9995)$, $i_{pa}(10^{-6}\ A) = -5.58\nu^{1/2}(V\ s^{-1})^{1/2} - 7.16(n = 5,\ \gamma = 0.9995)$, respectively, suggesting that the reaction is diffusion-controlled electrode reaction.

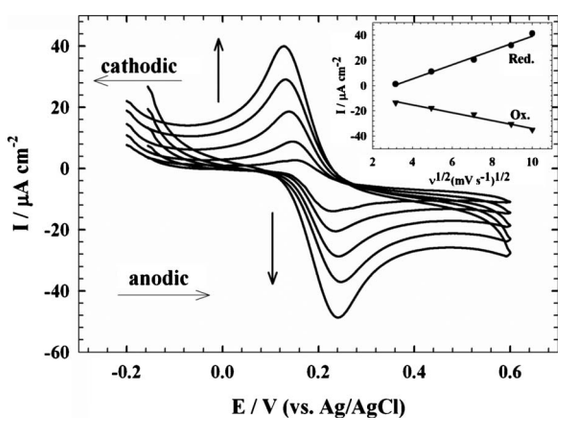

Figure 4. Cyclic voltammograms of 1.0 × 10^{-3} mol L^{-1} DA at the GNMCPE in 0.04 M B–R buffer pH 7.4 at 10, 25, 50, 80, and 100 mV s^{-1}.

Diffusion coefficients of DA in different buffer electrolytes.— The effect of changing the buffer type was studied on DA oxidation in the presence of B-R buffer pH 7.4 and PBS pH 7.4. It was clear that GNMCPE shows relatively better response in different types of buffers i.e., DA gave an oxidation peak current of 35.6 μA and 31.1 μA, in case of B-R buffer and PBS, respectively (Fig. 5A).

The relation between anodic peak current, i_{pa}(μA), and the diffusion coefficient of the electroactive species, D_0(cm^2 s^{-1}), is given by randles-Sevcik equation[43]:

$$i_{pa} = (2.69 \times 10^5)n^{3/2}AC_0^*D_0^{1/2}\nu^{1/2} \quad [1]$$

Where n is the number of electrons exchanged in oxidation at T = 298 K, A is the geometrical electrode area (0.0706 cm^2), C_0 is the analyte concentration (1 × 10^{-6} mol cm^{-3}) and ν is the scan rate (V s^{-1}).

The apparent diffusion coefficients, D_{app}, of DA in different electrolytes were calculated from CV experiments and the results were compared. In this study, the dependence of the anodic peak current density on the scan rate has been used for the estimation of the D_{app} of DA in different electrolytes according to the Randles–Sevcik equation. The calculated D_{app} values are 1.95 × 10^{-7} cm^2 s^{-1} for the bare CP electrode and 2.5 × 10^{-7} cm^2 s^{-1} for the GNMCPE in B–R buffer, while 1.93 × 10^{-7} cm^2 s^{-1} for the bare CP electrode and 2.4 × 10^{-7} cm^2 s^{-1} for GNMCPE in PBS. This indicated the enhanced mass transfer of the analyte molecules toward electrode surface from bulk solutions and fast electron transfer process of electrochemical oxidation of the analyte molecule at the electrode–solution interface.[44,45] Furthermore, it also showed that the redox reaction of the analyte species took place at the surface of the electrode under the control of the diffusion of the molecules from the solution to the electrode surface. The calculated D_{app} values for DA at the bare CP electrode and GNMCPE showed that Au particles improves the electron transfer kinetics at the electrode/solution interface, also changing the buffer type only caused very small changes.

Effect of electrodeposition time.— The electrodeposition time of gold was also studied as a factor that can affect the voltammetric determination of DA. The peak current increased with increasing the deposition time. When the deposition time reached 400 s, at the potential of −0.4 V (vs Ag/AgCl) in 6 mmol L^{-1} $HAuCl_4$, the GNMCPE surface gave the highest current response, so the opti-

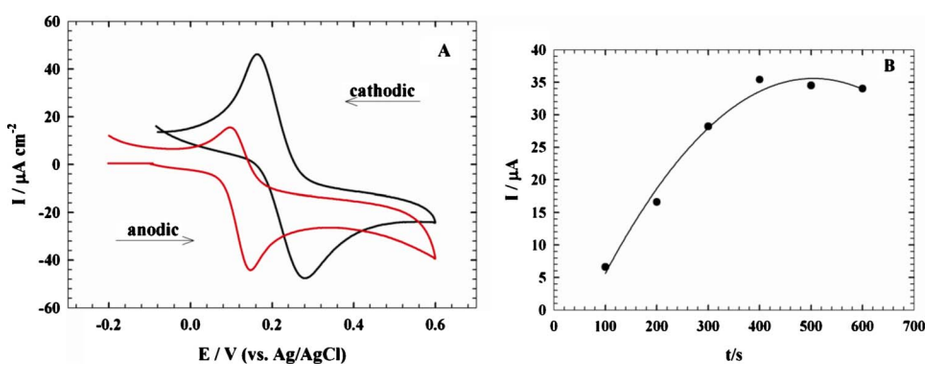

Figure 5. (Color online) (A) Cyclic voltammograms of 1.0 × 10^{-3} mol L^{-1} DA at the GNMCPE in different buffer types: B–R buffer pH 7.4 (—) and PBS pH 7.4 (red —). (B) Relation between the anodic peak current of 1.0 × 10^{-3} mol L^{-1} DA in 0.04 mol L^{-1} B–R buffer pH 7.4 at the GNMCPE and different electrodeposition times of gold nanoparticles: 100, 200, 300, 400, 500, and 600 s.

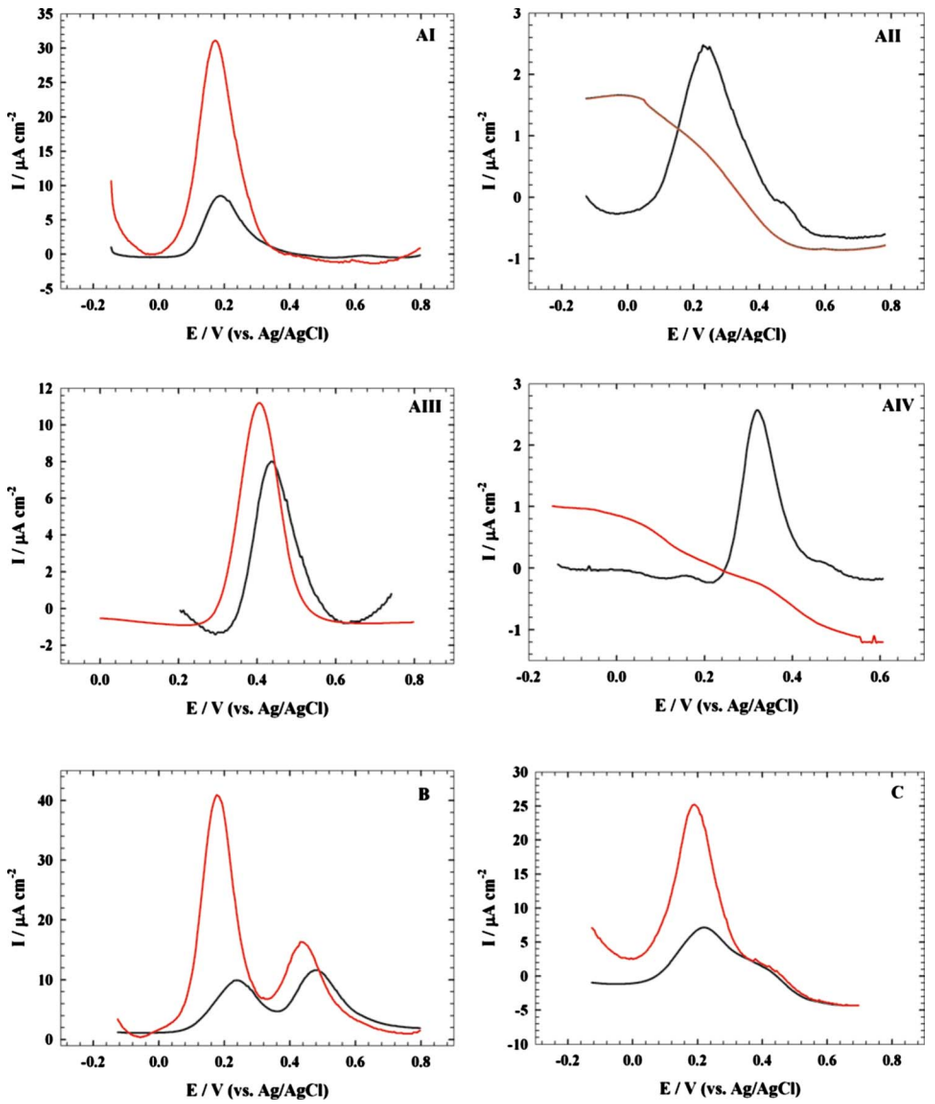

Figure 6. (Color online) (A) Differential pulse voltammograms obtained with the bare CP electrode (—) and GNMCPE (red —) in 1.0×10^{-5} mol L^{-1} of (I) DA, (II) AA, (III) ACOP, and (IV) UA in 0.04 mol L^{-1} B–R buffer pH 7.4 at a scan rate of 10 mV/s. (B) The differential pulse voltammograms obtained at bare CP (—) and GNMCPE (red —) electrodes for a mixture of 5 mmol L^{-1} DA + 5 mmol L^{-1} AA + 5 mmol L^{-1} ACOP in 0.04 mol L^{-1} B–R buffer pH 7.4 at a scan rate of 10 mV/s. (C) The differential pulse voltammograms obtained at bare CP (—) and GNMCPE (red —) electrodes for a mixture of 5 mmol L^{-1} DA + 5 mmol L^{-1} AA + 5 mmol L^{-1} UA in 0.04 mol L^{-1} B–R buffer pH 7.4 at a scan rate of 10 mV/s.

mum electrodeposition time used was 400 s (Fig. 5B). Studying the effect of accumulation time under open-circuit conditions showed that the peak current was independent on the accumulation time.

Interference studies.— Determination of DA in the presence of AA, UA, and ACOP.— The GNMCPE was used for the voltammetric detection of DA in the presence of ACOP and AA (mixture I), AA and UA (mixture II) in B–R buffer pH 7.4, the applied scan rate was 10 mV/s, using differential pulse voltammetry (DPV). Figure 6 (curve A-I) shows the DPV obtained with the bare CP electrode (solid line) and GNMCPE (dashed line) in 1.0×10^{-3} mol L^{-1} DA. The anodic peak current increased from 7.8 μA in the bare CP electrode to 31 μA in the GNMCPE, at the same oxidation potential. The determination of 1.0×10^{-3} mol L^{-1} AA on the bare CP-electrode gave a peak current at nearly the same oxidation potential as DA, causing an overlap of their responses when they were in the same mixture. This problem was solved by using GNMCPE, where the anodic peak current of AA disappears (curve A-II). The determination of 1.0×10^{-3} mol L^{-1} ACOP was also studied, where the peak current also increased upon using GNMCPE from 8.3 μA in the bare electrode to 10.95 μA (curve A-III). Curve A-IV shows that the oxidation potential of 1.0×10^{-3} mol L^{-1} UA almost occurred at the same potential as that of ACOP, while it disappeared where GNMCPE was used, which means that neither AA nor UA can interfere with DA when they are in a mixture using GNMCPE. Curve B shows the voltammograms of mixture I, under the optimum experimental conditions. As could be noticed, the response of mixture I in the bare CP electrode (solid line) shows two peaks, the first was for both DA and AA at 235 mV, while the second was for ACOP at 470 mV. Using GNMCPE (dashed line) two peaks were also obtained; the first one at 177 mV was for DA only, while the second peak at 420 mV was for ACOP, as illustrated in curve A. Curve C shows the voltammograms of mixture II, under the same optimum experimental conditions. As can be noticed in the bare CP electrode only one broad peak occurs for DA, UA, and AA, while in the GNMCPE one sharp peak with a relatively higher peak current for DA was observed as is illustrated in Fig. 6A.

The results of this study showed that the problem of interference of AA and UA for the determination of DA was eliminated by using the proposed modified electrode (GNMCPE) and that DA can also be determined in the presence of ACOP.

Determination of DA in the presence of high concentrations of AA and UA.— AA coexists with DA and UA in our body fluids and further its concentration is always much higher (10^{-4} mol L^{-1}) compared to that of DA and UA.[46] Therefore, the determination of DA in the presence of high concentration of AA and UA is very crucial from the clinical point of view. Figure 7 shows the DPV obtained at the GNMCPE for (5, 10, 15, 20, 30, 40, 50, 60, 80, and

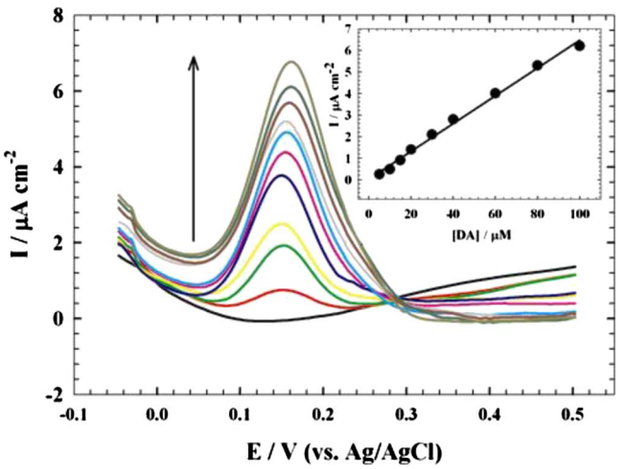

Figure 7. (Color online) The differential pulse voltammograms obtained at GNMCPE for (5, 10, 15, 20, 30, 40, 50, 60, 80, and 100 μmol L^{-1}) DA and 0.1 mmol L^{-1} UA in the presence of 5 mmol L^{-1} AA in B–R buffer pH 7.4 and a scan rate of 10 mV/s. The inset shows the corresponding calibration curve of DA.

100 μmol L^{-1}) DA and 0.1 mmol L^{-1} UA in the presence of 5 mmol L^{-1} AA in B–R buffer pH 7.4 and at a scan rate of 10 mV/s. Well-defined voltammetric signals for DA were obtained, and the inset illustrates the relation between the different concentrations of DA and the corresponding anodic peak currents, with a correlation coefficient of 0.9963. This indicated that the detection of very low concentrations of DA is possible even in the presence of a high concentration of AA and UA.

These results prove that GNMCPE is more selective for DA even in the presence of a high concentration of AA and UA. Moreover, the calibration equations for DA did not significantly change with increasing UA and AA. The elimination of the interference effect of AA and UA was due to the negatively charged surface of the GNMCPE in its anionic form at the working pH of 7.4, DA with pK_a of 8.9 was mainly in its cationic form which can be attracted to the electrode surface, while AA with pK_a of 4.2 [47] and UA with pK_a of 5.4 [47] ware in their anionic forms and were repelled by the negatively charged gold particles.[48]

EIS studies.— EIS is an effective tool for studying the interface properties of surface-modified electrodes. EIS data were obtained for the GNMCPE at an ac frequency varying between 0.1 Hz and 100 kHz with an applied potential in the region corresponding to the electrolytic oxidation of DA in B–R buffer pH 7.4. The data are presented as a relation between the impedance and the frequencies, the Bode plot (Fig. 8A) for the bare CP electrode (curve I) and GNMCPE (curve II). In all cases, the experimental data were compared to an "equivalent circuit" that used some of the conventional circuit elements, namely, resistance, capacitance, diffusion, and induction elements. The equivalent circuit is shown in Fig. 8C. In this circuit, R_u is the solution resistance, the constant phase element (CPE) represents mainly the electronic resistance, while CPE1 represents the predominant diffusion influence on the charge-transfer process, and α_1 and α_2 are their corresponding exponents. C_p and C_f represent the capacitance of the double layer.

Figure 8B (I) and (II) is the typical impedance spectrum pre-

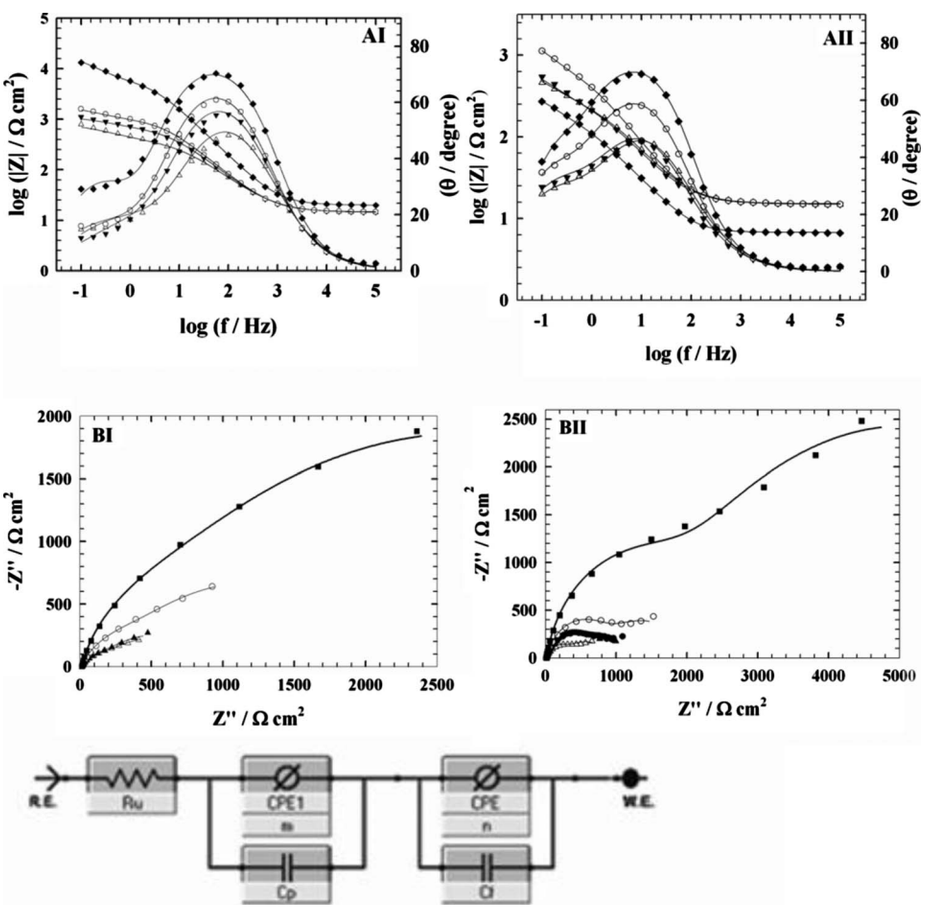

Figure 8. (A) The Bode plot for bare CP (I) and GNMCPE (II) electrodes at different oxidation potential values: 160 (△), 220 (▲), 280 (○), and 500 mV (■) (symbols and solid lines represent the experimental measurements and the computer fitting of impedance spectra, respectively). (B) The typical impedance spectrum presented in the form of the Nyquist plot for CP electrode (I) and GNMCPE (II) at different oxidation potential values: 160 (△), 220 (▲), 280 (○), and 500 mV (■) (symbols and solid lines represent the experimental measurements and the computer fitting of impedance spectra, respectively). (C) Equivalent circuit used in the fit procedure of the impedance spectra.

Table I. EIS fitting data corresponding to Fig. 8 (A) and (B).

Electrode	E (mV)	R_u (Ω cm^2)	CPE1 (kΩ cm^2)	α_1	C_p (μF cm^{-2})	CPE (kΩ cm^2)	α_2	C_f (μF cm^{-2})
Bare CP electrode	160	200.8	8.28	0.632	4.25	4.19	0.769	1.201
	220	204	9.21	0.651	3.686	7.517	0.817	1.201
	280	207	17.72	0.66	3.68	11.47	0.847	1.23
	500	208.3	95.54	0.777	2.563	25.73	0.887	1.016
GNMCPE	160	212.2	9.068	0.733	22.42	2.691	0.735	6.345
	220	215.3	9.871	0.755	24.56	2.602	0.735	7.248
	280	216	24.1	0.814	19.17	5.716	0.810	7.921
	500	218	57.6	0.904	14.89	12.13	0.868	7.358

sented in the form of the Nyquist plot for the CP electrode and GNMCPE, respectively. Figure 8B (I) include an ill-defined semicircle portion at higher frequencies corresponding to the electron transfer limited process. The semicircle diameter in the impedance spectrum equals the electron transfer resistance, R_{et}. This resistance controls the electron transfer kinetics of the redox probe at the electrode interface. Therefore, R_{et} can be used to describe the interface properties of the electrode. Figure 8B (II) proves that the model is represented as a two time constant. To obtain the detailed information of the impedance spectroscopy, a simple equivalent circuit model in Fig. 8C was used to fit the results (Fig. 8A). In Fig. 8B the CP electrode revealed a small semicircle domain (curve I), implying a low electron transfer resistance of the redox probe. After the CP electrode was modified with gold nanoparticles, a relatively smaller semicircle domain was obtained especially around the oxidation potential of DA (curve II), showing that the GNMCPE promotes more conductivity.

In the high frequency region of the spectra, pure resistive behavior could be noticed that was followed by a capacitive response as the frequency was shifted to relatively lower values. Table I lists the best fitting values calculated from the equivalent circuit for the impedance data of Fig. 8A. The average error (χ^2) of the fits for the mean error of modulus was in the range of $\chi^2 = (1.0–2.8) \times 10^{-2}$. The following observations and conclusions could be drawn from Table I: GNMCPE shows relatively increased values of the capacitive component compared to bare CP electrode indicating a more conducting character of the surface due to ionic adsorption at the electrode surface and the charge-transfer process. From the data indicated in Table I, the value of solution resistance, R_u, was almost constant within the limits of the experimental errors. However, the ionic/electronic charge-transfer resistance, CPE, shows a noticeable decrease in values in the GNMCPE to the CP electrode, which indicates less electronic resistance and more facilitation of charge transfer. CPE1 values did not differ considerably between the two electrodes. This was observed from the small difference in the apparent diffusion values of the two electrodes as was discussed in the Diffusion coefficients of DA in different buffer electrolytes section.

Analytical application.— Pulse voltammetric techniques such as DPV are effective and rapid electroanalytical techniques with well-established advantages, including good discrimination against background current and low detection limits

To prove the sensitivity of the GNMCPE toward the electrochemical measurement of DA, the effect of changing the concentration of DA in B–R buffer pH 7.4, using DPV mode, measured with GNMCPE working electrode was studied (Fig. 9A). The following are the parameters for the DPV experiments: $E_i = +200$ mV, $E_f = +1200$ mV, scan rate of 10 mV s^{-1}, pulse width of 25 ms, pulse period of 200 ms, and pulse amplitude of 10 mV. The corresponding calibration plot is given in Fig. 9B. The calibration plot was linearly related to the DA concentration over the ranges of 1.0×10^{-7} to 5.0×10^{-6} mol L^{-1} with the regression equation of $I_p(\mu A) = 0.727\ c(\mu mol\ L^{-1}) + 2.88 \times 10^5$ and 5.0×10^{-6} to 1.3×10^{-6} mol L^{-1} with the regression equation of $I_p(\mu A) = 2.23\ c(\mu mol\ L^{-1}) + 3.62 \times 10^4$ with correlation coefficients of 0.9995 and 0.9988 and the limits of detection (LOD) (signal to noise ratio of 3) was 5.9×10^{-9} and 8.2×10^{-8} mol L^{-1}, respectively. The LOD achieved using the surface suggested in the present work was within the lowest reported in the presence of uric and AAs as interfering species in biological fluids.[38,40]

Sample analysis in human serum.— To check, the possibility of applying the modified electrode (GNMCPE) to protein-free human serum samples, the calibration curves were obtained in spiked human serum samples. The determination of DA in spiked human serum could be achieved adopting the DPV mode in B–R buffer pH 7.4 as supporting electrolyte. The measurements of DA in human serum samples were performed as described in the Experimental section. The calibration equation parameters and necessary validation data were shown in Table II. At the bare CP electrode there is a shift in the oxidation peak potential to more positive values, which was not observed in the GNMCPE. Using either the DA stock solution or DA in the human serum gave nearly the same results. The developed methods were validated according to the standard proce-

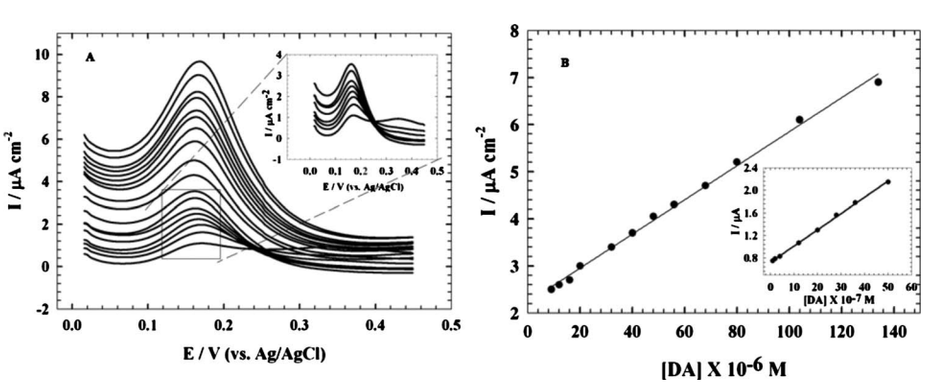

Figure 9. A The effect of changing the concentration of DA using differential pulse mode at GNMCPE in 0.04 mol L^{-1} B–R buffer pH 7.4 and a scan rate of 10 mV/s. The inset represents the differential pulse mode of the smaller concentration range. (B) The calibration curve of the oxidation peak current values of i_{pa} vs the concentration of DA. The inset represents the calibration curve of the smaller concentration range.

Table II. Regression data of the (A) first and (B) second linear range for quantitative determination of DA by DPV using (a) bare CP electrode, (b) GNMCPE in B–R buffer pH 7.4 and c) GNMCPE in human serum sample.

DA/pH 7.4 In case of	(a) Bare CP electrode	(b) GNMCPE	(c) Serum on GNMCPE
	(A) First linear range		
Measured oxidation potential (V)	1.61 → 2.11	1.71	1.78
Linearity range (mol L^{-1})	4×10^{-6}–9×10^{-5}	1×10^{-7}–6×10^{-6}	8×10^{-7}–7×10^{-6}
Slope (μA(mol L^{-1})$^{-1}$)	8.8×10^{4}	2.88×10^{5}	3.5×10^{5}
Intercept (μA)	0.1688	0.727	0.3796
Correlation coefficient	0.9935	0.9995	0.993
Standard error of slope	4.1×10^{2}	4.0×10^{3}	2.1×10^{3}
Standard error of intercept	1.97×10^{-2}	9.0×10^{-3}	8.44×10^{-3}
LOD (mol L^{-1})	1.6×10^{-7}	5.9×10^{-9}	4.2×10^{-9}
LOQ (mol L^{-1})	3.4×10^{-7}	1.9×10^{-8}	1.4×10^{-8}
	(B) Second linear range		
Measured oxidation potential (V)	2.11 → 2.88	1.71	1.78
Linearity range (mol L^{-1})	1.2×10^{-4}–8.8×10^{-4}	6×10^{-6}–1.3×10^{-4}	7×10^{-6}–1.3×10^{-4}
Slope (μA(mol L^{-1})$^{-1}$)	1.41×10^{3}	3.62×10^{4}	3.39×10^{4}
Intercept (μA)	1.0408	2.23	2.392
Correlation coefficient	0.9987	0.9988	0.998
Standard error of slope	23.3	7.0×10^{2}	7.0×10^{2}
Standard error of intercept	1.27×10^{-2}	4.39×10^{-2}	4.76×10^{-2}
LOD (mol L^{-1})	4.2×10^{-7}	8.2×10^{-8}	8.8×10^{-8}
LOQ (mol L^{-1})	1.4×10^{-6}	2.7×10^{-7}	2.9×10^{-7}

Table III. Evaluation of the accuracy and precision of the proposed method for the determination of (DA) in urine sample.

Concentration of DA added (mol L^{-1}) $\times 10^{-6}$	Concentration of DA found[a] (mol L^{-1}) $\times 10^{-6}$	Recovery (%)	Standard deviation $\times 10^{-8}$	SE[b] $\times 10^{-8}$	Confidence level[c] $\times 10^{-8}$
0.4	0.399	99.9	2.28	1.0	2.8
1.2	1.203	100.2	3.2	1.4	4.0
4.0	3.994	99.8	3.9	1.77	4.9
9.0	9.005	100	9.1	4.0	1.1

[a] Mean for five determinations.
[b] Standard error = SD/$\sqrt{n}$.
[c] CL confidence at 95% confidence level and 5 degrees of freedom (t = 2.776).

dures; also the LOD and limits of quantification (LOQ) are given in Table II. The LOD and LOQ were calculated from the peak current using the following equations

$$\text{LOD} = 3\ s/m$$

$$\text{LOQ} = 10\ s/m$$

where s is the standard deviation of the peak currents (three runs) and m is the slope of the related calibration curves. Both LOD and LOQ values confirmed the sensitivity of the proposed methods using GNMCPE.

Validation method in urine.— Validation of the procedure for the quantitative assay of the DA by performance characteristics method was examined in B–R buffer pH 7.4, at a scan rate of 10 mV/s using differential pulse technique. The calibration curve gave a straight line with correlation coefficient, r = 0.9996, the LOD is 2.6×10^{-8} mol L^{-1}. Four different concentrations on the calibration curve are chosen to be repeated for five times to evaluate the accuracy and precision of the proposed method, which is represented in (Table III).

Conclusion

In the present work, a biosensor based on CP electrode modified with gold nanoparticles was used for electrochemical determination of DA. The advantages of the gold nanoparticles enhanced the sensitivity of the CP electrode significantly. The experimental conditions such as pH, scan rate, accumulation time, types of electrolytes, and the deposition time were studied to find the highest sensitivity for the determination of DA. Under the optimum conditions, calibration plots for DA were linear in the ranges of 1.0×10^{-7} to 5.0×10^{-6} mol L^{-1} and 5.0×10^{-6} to 1.3×10^{-4} mol L^{-1} with correlation coefficients of 0.9995 and 0.9988 and detection limits of 5.9×10^{-9} and 8.2×10^{-8} mol L^{-1}, respectively. The results showed that the method was simple and sensitive enough for the determination of DA in human serum and urine samples with good precision and accuracy. The LOD achieved in this work is better than that or comparable to those reported for other surfaces including glassy carbon.[24,49,50]

In the present work, we demonstrated the selective determination of DA in the presence of AA and UA in 0.04 M B–R buffer (pH 7.4) using GNMCPE. The bare CP electrode failed to resolve the voltammetric signals of DA from AA and ACOP from UA. However, the GNMCPE enhanced the current signals of DA, while the oxidation peak currents of AA and UA disappeared.

Acknowledgment

The authors express their gratitude to the University of Cairo (Office of Vice President for Graduate Studies and Research) for providing partial financial support through "The Young Researchers' Program." We acknowledge the financial support by the National Organization for Drug Control and Research (NODCAR, Egypt).

University of Cairo assisted in meeting the publication costs of this article.

References

1. P. Damier, E. C. Hirsch, Y. Agid, and A. M. Graybiel, *Brain*, **122**, 1437 (1999).

2. C. Martin, *Chem. Br.*, **34**, 40 (1998).
3. J. W. Mo and B. Ogorevc, *Anal. Chem.*, **73**, 1196 (2001).
4. R. M. Wightman, L. J. May, and A. C. Michael, *Anal. Chem.*, **60**, 769A (1988).
5. H. A. Harper, *Detection of Dopamine Dynamics in the Brain, Review of Physiological Chemistry*, 13th ed., Lange Medical, Los Altos, CA (1977).
6. G. G. Guilbault, *Analytical Uses of Immobilized Enzymes*, pp. 1–453, Marcel Dekker, New York (1984).
7. F. Gerald and J. Combs, *The Vitamins: Fundamental Aspects in Nutrition and Health*, 2nd ed., Academic Press, San Diego, CA (1992).
8. J. Chen and C. S. Cha, *Electroanal. Chem.*, **463**, 93 (1999).
9. U. D. Pawar, A.V. Naik, A.V. Sulebhavikar, T. A. Datar, and K.V. Mangaonkar, *E-Journal of Chemistry*, **6**, 289 (2009).
10. J. Kulys, *Biosens. Bioelectron.*, **14**, 473 (1999).
11. C. M. V. B. Almeida and B. F. Giannetti, *Electrochem. Commun.*, **4**, 985 (2002).
12. D. Moscone, D. D. Ottavi, D. Compagnone, G. Palleschi, and A. Amine, *Anal. Chem.*, **73**, 2529 (2001).
13. N. S. Lawrence, R. P. Deo, and J. Wang, *Anal. Chem.*, **76**, 3735 (2004).
14. P. Tomčik, C. E. Banks, T. J. Davies, and R. G. Compton, *Anal. Chem.*, **76**, 161 (2004).
15. C. Ding, F. Zhao, R. Ren, and J. M. Lin, *Talanta*, **78**, 1148 (2009).
16. D. Tang, R. Yuan, and Y. Chai, *Anal. Chim. Acta*, **564**, 158 (2006).
17. M. B. González-García, C. Fernández-Sánchez, and A. Costa-García, *Biosens. Bioelectron.*, **15**, 315 (2000).
18. M. L. Mena, P. Yáñez-Sedeño, and J. M. Pingarrón, *Anal. Biochem.*, **336**, 20 (2005).
19. L. Agüí, J. Manso, P. Yáñez-Sedeño, and J. M. Pingarrón, *Sens. Actuators B*, **113**, 272 (2006).
20. L. Agüí, J. Manso, P. Yáñez-Sedeño, and J. M. Pingarrón, *Talanta*, **64**, 1041 (2004).
21. L. Agüí, C. Peña-Farfal, P. Yáñez-Sedeño, and J. M. Pingarrón, *Talanta*, **74**, 412 (2007).
22. H. Huang, P. Ran, and Z. Liu, *Bioelectrochemistry*, **70**, 257 (2007).
23. S. Upadhyay, G. R. Rao, M. K. Sharma, B. K. Bhattacharya, V. K. Rao, and R. Vijayaraghavan, *Biosens. Bioelectron.*, **25**, 832 (2009).
24. K. Márquez, R. Ortiz, J. W. Schultze, O. P. Márquez, J. Márquez, and G. Staikov, *Electrochim. Acta*, **48**, 711 (2003).
25. M. Moreno, E. Rincon, J. M. Pérez, V. M. González, A. Domingo, and E. Dominguez, *Biosens. Bioelectron.*, **25**, 778 (2009).
26. J. Wang, L. Wang, J. Di, and Y. Tu, *Talanta*, **77**, 1454 (2009).
27. Y. Ma, J. Di, X. Yan, M. Zhao, Z. Lu, and Y. Tu, *Biosens. Bioelectron.*, **24**, 1480 (2009).
28. Y. Wang, J. Deng, J. Di, and Y. Tu, *Electrochem. Commun.*, **11**, 1034 (2009).
29. N. Sakai, Y. Fujiwara, M. Arai, K. Yu, and T. Tatsuma, *J. Electroanal. Chem.*, **628**, 7 (2009).
30. L. Wang, W. Mao, D. Ni, J. Di, Y. Wu, and Y. Tu, *Electrochem. Commun.*, **10**, 673 (2008).
31. J. Wang, L. Wang, J. Di, and Y. Tu, *Sens. Actuators B*, **135**, 283 (2008).
32. R. Gao and J. Zheng, *Electrochem. Commun.*, **11**, 608 (2009).
33. F. Xiao, Z. Mo, F. Zhao, and B. Zeng, *Electrochem. Commun.*, **10**, 1740 (2008).
34. R. Zhang, G.-D. Jin, D. Chen, and X.-Y. Hu, *Sens. Actuators B*, **138**, 174 (2009).
35. R. Hosseinzadeh, R. E. Sabzi, and K. Ghasemlu, *Colloids Surf., B*, **68**, 213 (2009).
36. G.-Z. Hu, D.-P. Zhang, W.-L. Wu, and Z.-S. Yang, *Colloids Surf., B*, **62**, 199 (2008).
37. N. F. Atta, M. F. El-Kady, and A. Galal, *Sens. Actuators B*, **141**, 566 (2009).
38. N. F. Atta and M. F. El-Kady, *Sens. Actuators B*, **145**, 299 (2010).
39. N. F. Atta and M. F. El-Kady, *Talanta*, **79**, 639 (2009).
40. N. F. Atta, M. F. El-Kady, and A. Galal, *Anal. Biochem.*, **400**, 78 (2010).
41. J. Zheng and X. Zhou, *Bioelectrochemistry*, **70**, 408 (2007).
42. X. Jiang and X. Lin, *Anal. Chim. Acta*, **537**, 145 (2005).
43. N. Yang, Q. Wan, and J. Yu, *Sens. Actuators B*, **110**, 279 (2005).
44. W. Qijin, Y. Nianjun, Z. Haili, Z. Xinpin, and X. Bin, *Talanta*, **55**, 459 (2001).
45. V. S. Vasantha and S.-M. Chen, *J. Electroanal. Chem.*, **592**, 77 (2006).
46. T. Zetterström, T. Sharp, C. A. Marsden, and U. Ungerstedt, *J. Neurochem.*, **41**, 1769 (1983).
47. J. Li and X.-Q. Lin, *Anal. Chim. Acta*, **596**, 222 (2007).
48. Z. Nasri and E. Shams, *Electrochim. Acta*, **54**, 7416 (2009).
49. S. Thiagarajan, R.-F. Yang, and S.-M. Chen, *Bioelectrochemistry*, **75**, 163 (2009).
50. G. N. Kamau and J. F. Rusling, *Electroanalysis*, **6**, 445 (1994).